

Are Dawn Storms Jupiter's auroral substorms?

B. Bonfond^{1*}, Z. H. Yao^{2,1*}, G. R. Gladstone³, D. Grodent¹, J.-C. Gérard¹, J. Matar¹, B. Palmaerts¹, T. K. Greathouse³, V. Hue³, M. H. Versteeg³, J. A. Kammer³, R. S. Giles³, C. Tao⁴, M. F. Vogt⁵, A. Mura⁶, A. Adriani⁶, B. H. Mauk⁷, W. S. Kurth⁸, S. J. Bolton³

¹ Space Science, Technologies and Astrophysical Research Institute, Laboratory for Planetary and Atmospheric Physics, University of Liège, Liège, Belgium.

² Key Laboratory of Earth and Planetary Physics, Institute of Geology and Geophysics, Chinese Academy of Sciences, Beijing, China.

³ Southwest Research Institute, San Antonio, TX, USA.

⁴ National Institute of Information and Communications Technology, Tokyo, Japan.

⁵ Center for Space Physics, Boston University, MA, USA.

⁶ Institute for Space Astrophysics and Planetology, National Institute for Astrophysics, Rome, Italy.

⁷ Applied Physics Laboratory, Johns Hopkins University, Laurel, MD, USA.

⁸ Department of Physics and Astronomy, University of Iowa, Iowa City, IA, USA.

Are Dawn Storms Jupiter's auroral substorms?

B. Bonfond^{1*}†, Z. H. Yao^{2,1}†, G. R. Gladstone³, D. Grodent¹, J.-C. Gérard¹, J. Matar¹, B. Palmaerts¹, T. K. Greathouse³, V. Hue³, M. H. Versteeg³, J. A. Kammer³, R. S. Giles³, C. Tao⁴, M. F. Vogt⁵, A. Mura⁶, A. Adriani⁶, B. H. Mauk⁷, W. S. Kurth⁸, S. J. Bolton³

¹ Space Science, Technologies and Astrophysical Research Institute, Laboratory for Planetary and Atmospheric Physics, University of Liège, Liège, Belgium.

² Key laboratory of Earth and Planetary Physics, Institute of Geology and Geophysics, Chinese Academy of Sciences, Beijing, China.

³ Southwest Research Institute, San Antonio, TX, USA.

⁴ National Institute of Information and Communications Technology, Tokyo, Japan.

⁵ Center for Space Physics, Boston University, MA, USA.

⁶ Institute for Space Astrophysics and Planetology, National Institute for Astrophysics, Rome, Italy.

⁷ Applied Physics Laboratory, Johns Hopkins University, Laurel, MD, USA.

⁸ Department of Physics and Astronomy, University of Iowa, Iowa City, IA, USA.

*Correspondence to: b.bonfond@uliege.be.

†These authors contributed equally to this work.

Key points:

- Juno's observations provide the first global description of dawn storms in Jupiter's aurorae, from their initiation to their end.
- Examples of non-isolated dawn storms and smaller events named pseudo-dawn storms have been identified.
- Jovian dawn storms and terrestrial auroral substorms share many morphological and temporal characteristics.

Abstract

Dawn storms are among the brightest events in the Jovian aurorae. Up to now, they had only been observed from Earth-based observatories, only showing the Sun-facing side of the planet. Here we show for the first time global views of the phenomenon, from its initiation to its end and from the nightside of the aurora onto the dayside. Based on Juno's first 20 orbits, some patterns now emerge. Small short-lived spots are often seen for a couple of hours before the main emission starts to brighten and evolve from a straight arc to a more irregular one in the midnight sector. As the whole feature rotates dawn-ward, the arc then separates into two arcs with a central initially void region that is progressively filled with emissions. A gap in longitude then often forms before the whole feature dims. Finally, it transforms into an equatorward-moving patch of auroral emissions associated with plasma injection signatures. Some dawn storms remain weak and never fully develop. We also found cases of successive dawn storms within a few hours. Dawn storm thus share many fundamental features with the auroral signatures of the substorms at Earth. These findings demonstrate that, whatever their sources, mass and energy do not always circulate smoothly in planetary magnetospheres. Instead they often accumulate until the magnetospheres reconfigure and generate substorm-like responses in the planetary aurorae, although the temporal and spatial scales are different for different planets.

Plain language summary

Polar aurorae are a direct consequence of the dynamics of the plasma in the magnetosphere. The sources of mass and energy differ between the Earth's and Jupiter's magnetospheres, leading to fundamentally distinct auroral morphologies and very different responses to solar wind variations. Here we report on the imaging of all development stages of spectacular auroral events at Jupiter, called dawn storms, including, for the first time, their initiation on the nightside. Our

51 results reveal surprising similarities with auroral substorms at Earth, which are auroral events
52 stemming from explosive magnetospheric reconfigurations. Our results show that, despite their
53 major differences, the magnetospheres of the two planets can accumulate mass and energy in the
54 tail of their magnetosphere until they release them in an explosive manner. In spite of their
55 different scales and characteristics, this sudden reconfiguration of the magnetosphere triggers the
56 same types of substorm-like aurora in the polar regions of both the Earth and Jupiter, suggesting
57 that common universal processes are at play.

58 1. Introduction

59 The specificity of the dawn storms among the various auroral morphologies at Jupiter was
60 recognized as soon as the first high resolution ultraviolet (UV) images of the aurorae on Jupiter
61 became available (Gérard et al., 1994). As observed from the Hubble Space Telescope (HST),
62 having only access to the Earth-facing side of the aurora, they consist of a thickening and a major
63 enhancement of the brightness of the dawn arc of the main auroral emission (main oval). They
64 seem to last for at least 1-2 hours (Ballester et al., 1996), but given the typical length of HST
65 sequences is ~45 minutes, HST could not provide a complete and uninterrupted view of the
66 process. Dawn storms are also characterized by clear signatures of methane absorption,
67 indicating that the charged particles causing them can precipitate deep below the methane
68 homopause, with energies up to 460 keV (Gustin et al., 2006) in the case of electrons. Based on
69 the large HST observation campaign carried out in 2007, dawn storms appeared rare (3 cases out
70 of 54 observations) and occurred independently from the state of the solar wind (Nichols et al.,
71 2009). However, the dawn storm observed during the HST campaign supporting the Juno
72 mission as it approached Jupiter in 2016 occurred just as a coronal mass ejection hit Jupiter's
73 magnetosphere, re-igniting the debate on the relationship between dawn storms and solar wind

74 fluctuations (Kimura et al., 2017). So far, our understanding of dawn storms has been incomplete
75 mainly because we have been unable to observe the whole extent of the event, both temporally
76 and spatially. New data from the Juno mission reveal for the first time where and how the dawn
77 storms start and their consequences.

78 2. Image processing

79 Juno is a NASA New Frontiers spacecraft orbiting Jupiter since 4 July 2016. Its 53-day eccentric
80 polar orbit brings its perijove (PJ) to ~4000 km above the surface (1 bar level) at low latitudes.
81 This orbit allows its ultraviolet spectrograph (UVS) to acquire spectrally resolved images of the
82 polar aurorae from approximately 4 hours before the PJ (in the northern hemisphere) to
83 approximately 4 hours after PJ (in the southern hemisphere) with a ~1-hour interruption in
84 between during the closest approach at low latitude.

85 Juno-UVS is an imaging spectrograph operating in the 68 to 210 nm range (Gladstone et al.,
86 2017; Greathouse et al., 2013). Its dog-bone shaped slit is 7.2° long, 0.025° wide in the center
87 and 0.2° wide in the two extremities. The slit is generally oriented perpendicularly to the Juno
88 spin plane. However, a scan mirror located at the entrance of the instrument allows to shift the
89 field of view by up to $\pm 30^\circ$ from the spin plane. In the present work, only the data from the wide
90 parts of the slit are used, in order to optimize the signal to noise ratio. Moreover, the wavelength
91 range from 155 to 162 nm is selected in order to avoid regions affected by absorption of the UV
92 light by hydrocarbon molecules in the Jovian atmosphere (mostly methane) below 155 nm and
93 by reflected sunlight beyond 162 nm.

94 The calibrated data from Juno-UVS are available through the Planetary Data System in the
95 form of FITS files, which contain information about each event collected by the detector, such as
96 the time of the event, its position in X and Y on the detector, the corresponding wavelength, etc.

97 This first step of the processing consists of removing the noise due to particle (typically
98 relativistic electrons) penetrating into the instrument and impacting the detector from the signal
99 caused by UV photons. Contrary to photons, which are diffracted by the grating, penetrating
100 particles illuminate the detector in an almost homogenous fashion, as confirmed by observations
101 carried out in the radiation belts. We use a region between pixels 345 to 550 in the X direction
102 (corresponding to ~59.7 to 80.9 nm) and pixels 20 to 255 in the Y direction, which has a very
103 low effective area for extreme-UV photons (Hue et al., 2019), in order to estimate the count rate
104 per pixel due to radiation. This background noise is then removed from the photon illuminated
105 part of the detector.

106 The second step consists, for each detection event, of projecting the four corners of each
107 field of view element along the slit onto a Jupiter-shaped ellipsoid located 400 km above the 1-
108 bar level, using the SPICE kernels listed in the FITS file header. The brightness, derived from
109 the weighted counts and the exposure time, is then attributed to a quadrilateral formed by these 4
110 points. A map of the aurora is then progressively built by adding all the detected events for a
111 given Juno spin. Simultaneously, an exposure map, identifying the regions of the planet covered
112 by the instrument's field of view, is also constructed. Images of the whole aurorae are then
113 assembled by performing a weighted sum of the consecutive spins, with a higher weight being
114 attributed to the latest spin. Going back in time, each weighting coefficient is $1/10^{\text{th}}$ of the
115 previous one. We then divide the weighted sum of the counts with a weighted sum of the
116 exposure maps to derive our final brightness map. This method offers the best compromise
117 between the completeness of the auroral map and the dynamics of the auroral features. However,
118 since UVS cannot observe the whole aurora during a given spin during the perijove sequence, the

119 exact timing and duration of some transient events is uncertain, with temporal knowledge gaps of
120 30 seconds at best due to the spinning spacecraft.

121 Three main sources of uncertainty affect estimates of the total emitted power by the H₂
122 molecules in the UV: 1) systematic calibration uncertainties estimated on the order of 16%
123 (Gérard et al., 2020), 2) shot noise uncertainty, which depends on the number of counts in the
124 region of interest and is typically below 5% for the small spots and below 1% for the larger dawn
125 storm features and 3) the selection uncertainty, which depends on the way the region of interest
126 is defined and which may reach up to 15%. The quadratic sum of all these uncertainties can be
127 rounded to a reasonable value of 25% for power estimates.

128 3. Observations of dawn storms

129 3.1. Development sequence of typical dawn storms

130 For the first time, Juno-UVS granted us a complete and global picture of the auroral dawn
131 storms, from their initiation to their vanishing. Indeed, Juno captured views of dawn storms at
132 different stages of development in approximately half of the first 20 perijoves (Table 1).

133 For example, on 7 February 2018 (PJ11), Juno-UVS captured the initiation of a dawn storm from
134 low altitude (~43000 km) above the north pole, thus allowing unprecedented high spatial
135 resolution observations (Figure 1). Around 13:06 UT, the event started with a relatively bright
136 midnight arc (~2000 kR). Then a few spots began to appear poleward of this arc, creating a
137 string of approximately a dozen spots within 14 minutes, each one forming ~1000 km dusk-ward
138 of the previous (Figure 2). These spots are approximately ~1000 km long (in the north-south
139 direction) and ~150 km wide, which corresponds to the projection of the instrumental point
140 spread function (PSF) on the planet. Hence, the apparent North-South extension probably result
141 from the asymmetry of the PSF. They each typically emit ~1GW of total power and appear with

142 a peak brightness of ~ 800 kR. Using the flux mapping method of (Vogt et al., 2015), but with
143 JRM09 (Connerney et al., 2018) as an internal field model, these spots map to a distance of 65-
144 110 Jovian radii (R_J) and a local time range between 22:40 UT and 23:45 UT, which broadly
145 corresponds to the X-line, where magnetotail reconnections take place (Vogt et al., 2010). When
146 mapped in the magnetosphere, the inter-spot distance corresponds to $1-2^\circ$ of longitude, or to a
147 mapped distance of 6-7 R_J . The distance between the mapped locations of the first (and dawn-
148 most) and last (and dusk-most) spots is about $42 R_J$ ($\sim 3 \cdot 10^6$ km), and the associated propagation
149 speed would be on the order of 3600 km/s in the azimuthal direction. If we focus on the brightest
150 central spots, this apparent mapped azimuthal velocity reaches 10 000 km/s. If these spots indeed
151 correspond to magnetic reconnection on the X-line, it is however quite likely that these high
152 values do not correspond to any physical velocity in the magnetosheet, and that the time interval
153 rather corresponds to a phase delay. Furthermore, these numbers should be considered as rough
154 estimates only, since 1) the mapping uncertainty strongly increases with radial distance, and 2)
155 any static mapping model is inaccurate, whatever the planet, during magnetospheric
156 reconfiguration events. Even though the spin modulated sampling rate of UVS does not allow
157 for easy monitoring, individual spots appear to vanish after a few minutes. These short-lived
158 spots may be similar to the midnight spots occasionally observed from the Hubble Space
159 Telescope at the limb of the planet (Grodent et al., 2004; Radioti et al., 2011). Another example
160 of transient bright spots was found during PJ16 (see Figure S1).

161 Two hours later, Juno was located over the southern hemisphere when the main emission began
162 to brighten and broaden irregularly, forming a bead-like pattern in the same midnight sector
163 (Figure S2). Fly-bys carried out at lower altitude during this phase of the dawn storm, such as
164 during PJ3 at 15:37 UT, render this pattern, with beads with ~ 1500 km ($\sim 2^\circ$) spacing, even more

165 obvious. Once mapped into the magnetodisk, these beads appear to originate from a region ~ 50
166 R_J from Jupiter and are azimuthally separated by $\sim 8 R_J$ (3° of longitude) in the magnetospheric
167 local time range between $\sim 1:45$ and $\sim 3:00$ LT. Hence, the enhancement of the main emission,
168 leading to the full-fledged dawn storm, actually started around magnetospheric midnight. This
169 feature then slowly migrated to the dawn sector at a pace corresponding to $\sim 25\%$ of corotation
170 with the planet. Around 16:22 UT, the main arc split into two parts, with one moving ~ 2500 km
171 towards the pole while the other remain relatively still. Because it is likely that these auroral
172 features arise from a reconfiguration of the magnetic field, static magnetic field mapping models
173 would most probably provide misleading results. The whole feature continued to rotate,
174 progressively accelerating towards co-rotation with the magnetic field as the dawn storm
175 developed. Around 17:15 UT, the feature appeared to split, but longitudinally this time. The
176 gap extends over $\sim 10^\circ$ of longitude in the upper atmosphere. At its peak, the total power
177 reached 850 GW, which is among the brightest events observed during Juno's first 20 orbits (see
178 Table 1). The UVS perijove observations ended at 18:50 UT, even though the event was still
179 ongoing.

180 On 19 May 2017 (PJ6), the Juno-UVS observations missed the beginning of an event, but
181 allowed us to examine the next phases. After the broadening and the latitudinal splitting of the
182 main emission, the outer-most arc transformed into large patches. On the same day, subsequent
183 HST images acquired with the Space Telescope Imaging Spectrograph (STIS) confirmed that the
184 patches continued their evolution, forming latitudinally extended fingers slowly expanding
185 equatorward. Such features have been associated with large and fresh plasma injection signatures
186 (Dumont et al., 2018). While such a connection between dawn storms and large injection
187 signatures has been proposed previously, based on the simultaneous presence of a dawn storm

188 and large injection signatures on the same image (Gray et al., 2016; Grodent et al., 2018), this
189 long and continuous set of observations from Juno and Hubble is the first to clearly demonstrate
190 the transition from one into the other. It should also be noted that some (less intense) injection
191 signatures can also appear independently from dawn storms, as was observed during PJ1 for
192 example (Bonfond et al., 2017).

193 3.2. Non-isolated dawn storms

194 Juno-UVS observations of dawn storms show that they sometimes occur as a series, rather than
195 isolated events. For example, on 27 March 2017 (PJ5), a first dawn storm was ongoing when the
196 observations started at 03:57 UT and was finished by approximately 06:51 UT, after which a
197 second one was observed peaking around 08:14 UT (Figure 3). In other cases, there appears to be
198 no gap between consecutive events. For example, during PJ3 (11 December 2016), the dawn
199 storm expansion phase seemed to never really stop, continuously going on at the same local time.
200 The dawn storm was first observed with the apparition of beads around 15:21 UT, as Juno was
201 flying over the northern hemisphere, and continued until auroral observations were interrupted
202 by Juno's low latitude fly-by. When observations of the southern hemisphere started over, a
203 dawn storm was still ongoing and this continued until the end of the sequence at 22:01 UT, with
204 the emitted power increasing around the end.

205 3.3. Pseudo-dawn storms

206
207 During PJ16 (29 October 2018), Juno-UVS observed the development of a particularly limited
208 dawn storm-like event (Figure 4). Around 20:19 UT, the instrument captured the appearance of
209 three transient (~6 minutes) spots poleward of the midnight arc of the main emission. Moreover,
210 the midnight arc itself was fainter than during PJ11 and the number of spots was also smaller.

211 The brightness of the enhanced the dawn arc of the main emission observed at 23:39 UT was
212 fairly dim (~ 500 kR), and the area concerned with the enhancement was limited ($\sim 10^\circ$ in
213 longitude). While the sequence of events is similar to the one observed on PJ11, which is why
214 we identify it here as a dawn storm, it would probably not have qualified as a dawn storm in
215 previous studies, due to its limited extent and brightness. This reason, together with the fact that
216 Juno observes the whole auroral region, including the nightside where dawn storms arise, almost
217 continuously for ~ 8 hours explains the discrepancy between our detection rate and the one
218 deduced from HST, which only focused on the expansion phase. The second dawn storm on PJ5
219 is another example of such a limited dawn storm (Figure 3, top right panel).

220

221 4. Discussion

222

223 Put together, the Juno-UVS observations paint a brand new picture of dawn storms. They consist
224 of a 5-10 hour long chain of events, starting with the transient spots (Figure S1), followed 2-3
225 hours hours later by the formation of bead-like features on the midnight part of the main
226 emissions (Figure S2). This time delay between events taking place at 90 and 50 R_J , respectively,
227 suggests a propagation speed of 250-400 km/s, which is consistent with estimates of the Alfvén
228 velocity in the plasma sheet (Manners et al., 2018). This is followed by an expansion phase,
229 during which the main emission brightens, expands, thickens and forks into two branches (Figure
230 S3). This chain of events is very similar to the one observed during terrestrial auroral substorms
231 (Figure 5). Substorms are global reconfigurations of the magnetosphere during which the
232 magnetic energy stored in the magnetotail is converted into particle energy, which lead to
233 spectacular auroral brightening in nightside polar regions which generally follow a well-
234 established sequence of features (Akasofu, 2013). The transient spots observed in Jupiter's

235 aurora share several morphological and temporal characteristics with transient meso-scale
236 features on Earth, sometimes associated with poleward boundary intensifications (PBIs) and
237 sometimes with streamers (Forsyth et al., 2020). Both are often observed before the substorm
238 onset (Nishimura et al., 2011), even if the exact relationship between streamers and substorms is
239 disputed (Miyashita & Ieda, 2018). Both phenomena are associated with reconnection in the
240 magnetotail and the subsequent inward flow of plasma and dipolarizing field lines
241 (Angelopoulos et al., 2008). At Jupiter, the tentative connection between magnetotail
242 reconnection and dawn storm has been evoked by several authors (Ballester et al., 1996; Ge et
243 al., 2010). Recently, the most compelling examples of such a connection come from
244 contemporaneous in situ particle and fields measurements by Juno and HST images of the aurora
245 (Yao et al., 2020). These observations show large reconnection signatures on magnetic field lines
246 mapping poleward of a dawn storm and then dipolarization signatures preceding auroral injection
247 signatures. The pre-expansion beads observed in the context of terrestrial substorms (Henderson,
248 2009) are associated with plasma instabilities in the near magnetotail, such as the ballooning
249 instability (Yao et al., 2017). The expansion phases of Jupiter’s dawn storms and the Earth’s
250 substorms also share fundamental similarities, and the latter is known to be associated with a
251 dipolarization/current disruption in the magnetosphere. In particular, the apparition of a
252 bifurcated oval at Jupiter resembles terrestrial bulge-type aurora observed during substorms
253 (Gjerloev et al., 2007, 2008). Finally, the auroral patches in the equatorward emissions manifest
254 massive plasma injections (Figure S6). Plasma injections in the inner terrestrial magnetosphere
255 are indeed observed by in situ instruments during substorm events (Gabrielse et al., 2019) and
256 they can also give rise to equatorward moving auroral enhancements (Sergeev et al., 2010). One

257 notable difference is that auroral substorms do not rotate with the Earth, but evolve in fixed local
258 time, i.e., around midnight (with a slight preference at pre-midnight (Gjerloev et al., 2004)).

259 At Earth, substorms do not always occur as isolated events. Instead, multiple substorm
260 expansions can happen consecutively (Liou et al., 2013). A similar behavior is observed for
261 dawn storms at Jupiter. The occurrence of successive dawn storms separated by a delay of a few
262 hours could explain why images of dawn storms from HST often display large injection
263 signatures in the post-noon sector (Gray et al., 2016; Grodent et al., 2018). Furthermore, (Yao et
264 al., 2020) suggest that successive dawn storms are responsible for the multiple injection auroral
265 structures.

266 Terrestrial substorms vary considerably in intensity and those which could not fully develop are
267 called pseudo-breakups (Pulkkinen et al., 1998). The event observed during PJ16 (29 October
268 2018) was limited to a small intensification, which might be analogous to terrestrial pseudo-
269 breakups (Fig. S2).

270 The orientation of the interplanetary magnetic field (and, to a lesser extent, the dynamic pressure
271 of the solar wind) controls the occurrence and intensity of Earth substorms (Kullen & Karlsson,
272 2004). Unfortunately, these solar wind parameters are difficult to obtain at Jupiter while Juno
273 carries out its perijove observations. Therefore, we used the propagation model from Tao et al.
274 (2005), which relies on measurements acquired at one astronomical unit from the Sun (from
275 either the OMNI data or the Stereo A spacecraft) to estimate the solar wind velocity and dynamic
276 pressure at Jupiter when Jupiter and the observatory are sufficiently well aligned ($<40^\circ$) (Figures
277 S6-S8). Most dawn storms for which such an estimate was possible (i.e. PJ5, PJ9, PJ14 and
278 PJ20) happened more than 2 days away from any solar wind enhancement, which confirms that
279 dawn storm may occur during relaxed solar wind conditions. However, they can also occur at

280 times closer to a solar wind enhancement (e.g. PJ1, PJ6 and PJ16), suggesting that solar wind
281 shocks do not necessarily prevent their occurrence. The comparison of the location of the
282 magnetopause measured by Juno and the aurora observed by HST also suggests that dawn storms
283 happen independently of the state of compression of the magnetosphere and are most probably
284 internally driven, contrary to the global main emission brightenings, which only occur in the
285 compressed state (Yao et al., 2020).

286 Regardless of the similarities between terrestrial substorms and Jovian dawn storms, it is also
287 important to stress the major differences between the Earth's and Jupiter's magnetospheres
288 (Mauk & Bagenal, 2013). The first is dominated by its interaction with the solar wind, and
289 magnetic reconnections on the dayside magnetopause drive the plasma convection in the
290 magnetosphere through the so-called Dungey cycle (Dungey, 1961). On the other hand, the
291 Jovian magnetosphere is inflated with plasma originating from the volcanic moon Io and the
292 rotation of the planet controls the motion and the energization of the magnetospheric plasma.
293 The mechanism through which the mass injected at Io is ultimately released via reconnection on
294 closed field lines is called the Vasyliunas cycle (Kronberg et al., 2007; Vasyliunas, 1983).
295 Reconnection on the dayside magnetopause, while it does exist at Jupiter (Ebert et al., 2017),
296 cannot open a significant amount of flux (Desroche et al., 2012; Masters, 2017), leading to a very
297 different type of magnetospheric topology (Zhang et al., 2020). By comparing the occurrence of
298 magnetotail reconnection and plasmoid release to predictions of the solar wind input, (Vogt et
299 al., 2019) showed that these large scale reconfigurations of the magnetotail were mostly
300 independent from solar wind compression.

301 However, regardless of the different reasons for the loading, in both cases plasma and energy
302 regularly accumulates within the system, which grows increasingly unstable, especially in the

303 midnight magnetotail where the field lines are the most elongated. While the long term
304 (~months) global evolution of the position of the main auroral emissions has been attributed to
305 the variations of the mass output from Io (Bonfond et al., 2012), the shorter term variations of its
306 position at different local times are poorly understood. Hence, since its typical location at
307 midnight for the various System III longitudes is unknown, we were unable to identify any
308 equatorward departure from it, as typically observed for the terrestrial growth phase auroral arcs.

309 Such a stretching of the field lines provides favorable conditions for reconnection to occur. At
310 Earth, such reconnection closes the magnetic field lines open to the solar wind in the
311 magnetotail, while at Jupiter, reconnection is internally driven (Ge et al., 2010; Kronberg et al.,
312 2005; Vogt et al., 2019; Woch et al., 2002) and is expected to take place on closed field lines. In
313 the middle magnetosphere, various plasma instabilities may occur, such as ballooning instability
314 (Hameiri et al., 1991; Kalmoni et al., 2018; Oberhagemann & Mann, 2020), cross-field current
315 instability (Lui et al., 1991) or shear flow-interchange instability (Derr et al., 2020). Since the
316 magnetic field lines in Jupiter's outer magnetosphere are also highly stretched, and the
317 magnetosphere consists of more energetic ions than the Earth's magnetotail, many plasma
318 instabilities identified in Earth's magnetotail would likely take place in Jupiter's outer
319 magnetosphere. Such instabilities can then lead to a disruption of the azimuthal currents in the
320 middle magnetosphere and a dipolarization of the field lines. While the dipolarizing field lines
321 would remain in the night sector at Earth, they would be progressively swept away in azimuthal
322 direction by the planetary rotation at Jupiter as they progress inward. This makes studies of east-
323 ward or west-ward expansion of the dawn storm almost impossible at Jupiter, because the exact
324 longitudinal expansion would be very difficult to disentangle from partial corotation. These
325 processes would also bring hot and sparse plasma from the outer magnetosphere further into the

326 system and energize it, forming plasma injections (Yao et al., 2020). Their study also shows that
327 dipolarization at Jupiter may corotate with the planet, as a counterpart of corotating auroral
328 injection.

329 The above explanation probably gives the impression that the dawn storm auroral sequence
330 suggests that the magnetotail reconfigurations at Jupiter are systematically “outside-in” in nature
331 rather than “inside-out”. Here the outside and inside represent relatively further or closer to the
332 planet. For the terrestrial case, this debate has been raging for years despite the flotilla of
333 dedicated spacecraft cruising in the magnetosphere and we certainly would not want to suggest
334 that with the few cases presented here, Juno has single handedly solved the problem at Jupiter.
335 As a possible counter-example, the auroral observations during PJ1 with Juno-UVS have shown
336 the progressive development of injection signature all around the pole before a poleward
337 protrusion (the shape of which may be reminiscent of omega bands at Earth) appeared on the
338 midnight arcs of the main emissions (Bonfond et al., 2017). It then took 2 hours for bead-like
339 features and then a dawn storm expansion phase to appear on infrared images (see supplemental
340 material S9). Contrary to the other sequences discussed here, this particular one thus suggests
341 that magnetospheric instabilities appeared closer to Jupiter before they developed further out.
342 Some studies at Earth also suggested that both situations might appear at Earth (Murphy et al.,
343 2014). Rather than a unique causal process leading to systematic chain of events, a possible
344 interpretation is that the accumulation of mass and energy makes the different regions of the
345 magnetosphere progressively susceptible to different types of plasma instabilities (including, at
346 places, reconnection). Once one of these regions reaches the instability threshold, the generated
347 disturbance propagates to the other region, making their own collapse more likely.

348 While they have some unique characteristics as well, the magnetosphere and aurorae at Saturn
349 are generally understood as representing an intermediate case between the Earth and Jupiter.
350 Indeed several lines of evidence (Bader et al., 2019) show that Saturn supports a combination of
351 Vasyliunas and rotating Dungey cycles (Cowley et al., 2005). It is thus less of a surprise to find
352 similar auroral features, such as transpolar arcs (Radioti et al., 2013) or auroral beads (Radioti et
353 al., 2019) in both the terrestrial and the Kronian aurorae. On the other hand, both observational
354 and theoretical arguments indicate that the overall dynamics of the plasma in the two
355 magnetospheres are fundamentally different (Bagenal & Delamere, 2011; Delamere et al., 2015;
356 Louarn et al., 2000), one being mostly externally driven and the other being mostly internally
357 driven. It is thus remarkable that universal processes releasing the accumulated matter and
358 energy from the systems generate strikingly similar auroral signatures.

359 Summary and conclusions

360 Freed from all the biases related to Earth-based observations, we detected dawn storms in
361 approximately half of the Juno perijove sequences (10 dawn storm observations over 19
362 orbits – no observations were carried out during PJ2). This is due to three factors: 1) longer
363 observations, providing additional chances to catch dawn storm at any stage of their
364 development, 2) a view of the nightside, where the dawn storms actually form and 3) a
365 looser definition of the dawn storm, which is no longer restricted to the brighter examples.
366 Moreover, the occurrence of dawn storms appears independent of the arrival of a solar
367 wind compression region at Jupiter.

368 While every feature has not been observed in each case, the dawn storms appear to follow
369 a systematic sequence of events (Figure 5), some of which are being reported here for the

370 first time. A dawn storm precursor appears to be the appearance of a series of transient
371 spots separated by ~ 1000 km, mapping to the pre-midnight sector. Approximately 2 to 3
372 hours later, the midnight section of the main emission starts to brighten, often forming
373 regularly spaced (~ 1500 km apart) beads. The arc further brightens and expands in
374 longitude as it progressively starts to co-rotate with the planet and to move towards the
375 dawn side. Then it bifurcates, with a branch moving poleward. The void between the arcs
376 then fills progressively as the arcs broaden in latitude. A longitudinal gap also generally
377 forms within the feature. Finally, the whole feature dims and the equatorward part of the
378 dawn storms evolves as an equatorward patch of emission associated with plasma
379 injection signatures, providing a direct link between dawn storms and some plasma
380 injection signatures.

381 Many of these auroral forms at Jupiter resemble meso-scale (Forsyth et al., 2020) and large
382 scale auroral forms observed during substorms at Earth. Furthermore, we found cases of
383 consecutive dawn storms occurring within a few hours, similar to the non-isolated
384 substorms at Earth. We also found cases of particularly weak dawn storm, reminiscent of
385 pseudo-breakups at Earth.

386 The magnetospheric processes associated with substorm magnetotail reconfigurations,
387 such as tail reconnection, dipolarization or hot plasma injection have also been observed at
388 Jupiter (Kronberg et al., 2005; Louarn et al., 2014; Mauk et al., 1997; Vogt et al., 2010; Woch
389 et al., 2002). The connection between these processes and dawn storms, was proposed
390 based on measurements from either in situ magnetic field or auroral images (Ge et al.,
391 2010; Kimura et al., 2017), and was later confirmed by contemporaneous measurements

392 from Juno and HST (Yao et al., 2020), associated with dawn storms. Despite the fact that the
393 mass and energy loading in the magnetotail at Earth and Jupiter are very different, the
394 evidence presented here show that the auroral signatures of the processes releasing them
395 at Jupiter are remarkably similar to terrestrial auroral substorm.

396

397
398
399
400
401
402
403
404
405
406
407
408
409
410
411
412
413
414
415
416
417
418
419
420
421
422
423

References

- Adriani, A., Filacchione, G., Di Iorio, T., Turrini, D., Noschese, R., Cicchetti, A., et al. (2017). JIRAM, the Jovian Infrared Auroral Mapper. *Space Science Reviews*, 213(1), 393–446. <https://doi.org/10.1007/s11214-014-0094-y>
- Akasofu, S.-I. (2013). Auroral Morphology: A Historical Account and Major Auroral Features During Auroral Substorms. In *Auroral Phenomenology and Magnetospheric Processes: Earth And Other Planets* (pp. 29–38). American Geophysical Union (AGU). <https://doi.org/10.1029/2011GM001156>
- Angelopoulos, V., McFadden, J. P., Larson, D., Carlson, C. W., Mende, S. B., Frey, H., et al. (2008). Tail Reconnection Triggering Substorm Onset. *Science*, 321(5891), 931–935. <https://doi.org/10.1126/science.1160495>
- Bader, A., Badman, S. V., Cowley, S. W. H., Yao, Z. H., Ray, L. C., Kinrade, J., et al. (2019). The Dynamics of Saturn’s Main Aurorae. *Geophysical Research Letters*, 46(17–18), 10283–10294. <https://doi.org/10.1029/2019GL084620>
- Bagenal, F., & Delamere, P. A. (2011). Flow of mass and energy in the magnetospheres of Jupiter and Saturn. *Journal of Geophysical Research: Space Physics*, 116(A5). <https://doi.org/10.1029/2010JA016294>
- Ballester, G. E., Clarke, J. T., Trauger, J. T., Harris, W. M., Stapelfeldt, K. R., Crisp, D., et al. (1996). Time-Resolved Observations of Jupiter’s Far-Ultraviolet Aurora. *Science*, 274, 409–413. <https://doi.org/10.1126/science.274.5286.409>
- Bonfond, B., Grodent, D., Gérard, J.-C., Stallard, T., Clarke, J. T., Yoneda, M., et al. (2012). Auroral evidence of Io’s control over the magnetosphere of Jupiter. *Geophysical Research Letters*, 39(1). <https://doi.org/10.1029/2011GL050253>
- Bonfond, B., Gladstone, G. R., Grodent, D., Greathouse, T. K., Versteeg, M. H., Hue, V., et al. (2017). Morphology of the UV aurorae Jupiter during Juno’s first perijove observations. *Geophysical Research Letters*, 44(10), 4463–4471. <https://doi.org/10.1002/2017GL073114>
- Connerney, J. E. P., Kotsiaros, S., Oliverson, R. J., Espley, J. R., Joergensen, J. L., Joergensen, P. S., et al. (2018). A New Model of Jupiter’s Magnetic Field From Juno’s First Nine Orbits. *Geophysical Research Letters*, 45(6), 2590–2596. <https://doi.org/10.1002/2018GL077312>

424 Cowley, S. W. H., Badman, S. V., Bunce, E. J., Clarke, J. T., Gérard, J.-C., Grodent, D., et al. (2005). Reconnection
425 in a rotation-dominated magnetosphere and its relation to Saturn's auroral dynamics. *Journal of*
426 *Geophysical Research: Space Physics*, 110(A2). <https://doi.org/10.1029/2004JA010796>

427 Delamere, P. A., Bagenal, F., Paranicas, C., Masters, A., Radioti, A., Bonfond, B., et al. (2015). Solar Wind and
428 Internally Driven Dynamics: Influences on Magnetodiscs and Auroral Responses. *Space Science Reviews*,
429 187(1), 51–97. <https://doi.org/10.1007/s11214-014-0075-1>

430 Derr, J., Horton, W., & Wolf, R. (2020). Shear Flow-Interchange Instability in Nightside Magnetotail as Proposed
431 Cause of Auroral Beads as a Signature of Substorm Onset. *Journal of Geophysical Research: Space*
432 *Physics*, 125(1), e2019JA026885. <https://doi.org/10.1029/2019JA026885>

433 Desroche, M., Bagenal, F., Delamere, P. A., & Erkaev, N. (2012). Conditions at the expanded Jovian magnetopause
434 and implications for the solar wind interaction. *Journal of Geophysical Research: Space Physics*, 117(A7).
435 <https://doi.org/10.1029/2012JA017621>

436 Dumont, M., Grodent, D., Radioti, A., Bonfond, B., Roussos, E., & Paranicas, C. (2018). Evolution of the Auroral
437 Signatures of Jupiter's Magnetospheric Injections. *Journal of Geophysical Research: Space Physics*, 0(0).
438 <https://doi.org/10.1029/2018JA025708>

439 Dungey, J. W. (1961). Interplanetary Magnetic Field and the Auroral Zones. *Physical Review Letters*, 6(2), 47–48.
440 <https://doi.org/10.1103/PhysRevLett.6.47>

441 Ebert, R. W., Allegrini, F., Bagenal, F., Bolton, S. J., Connerney, J. E. P., Clark, G., et al. (2017). Accelerated flows
442 at Jupiter's magnetopause: Evidence for magnetic reconnection along the dawn flank. *Geophysical*
443 *Research Letters*, 44(10), 4401–4409. <https://doi.org/10.1002/2016GL072187>

444 Forsyth, C., Sergeev, V. A., Henderson, M. G., Nishimura, Y., & Gallardo-Lacourt, B. (2020). Physical Processes of
445 Meso-Scale, Dynamic Auroral Forms. *Space Science Reviews*, 216(4), 46. [https://doi.org/10.1007/s11214-](https://doi.org/10.1007/s11214-020-00665-y)
446 [020-00665-y](https://doi.org/10.1007/s11214-020-00665-y)

447 Gabrielse, C., Spanswick, E., Artemyev, A., Nishimura, Y., Runov, A., Lyons, L., et al. (2019). Utilizing the
448 Heliophysics/Geospace System Observatory to Understand Particle Injections: Their Scale Sizes and
449 Propagation Directions. *Journal of Geophysical Research: Space Physics*, 124(7), 5584–5609.
450 <https://doi.org/10.1029/2018JA025588>

451 Ge, Y. S., Russell, C. T., & Khurana, K. K. (2010). Reconnection sites in Jupiter's magnetotail and relation to
452 Jovian auroras. *Planetary and Space Science*, 58(11), 1455–1469. <https://doi.org/10.1016/j.pss.2010.06.013>

453 Gérard, J. C., Grodent, D., Dols, V., Prangé, R., Waite, J. H., Gladstone, G. R., et al. (1994). A Remarkable Auroral
454 Event on Jupiter Observed in the Ultraviolet with the Hubble Space Telescope. *Science*, 266(5191), 1675–
455 1678. <https://doi.org/10.1126/science.266.5191.1675>

456 Gérard, J.-C., Gkouvelis, L., Bonfond, B., Grodent, D., Gladstone, G. R., Hue, V., et al. (2020). Spatial distribution
457 of the Pedersen conductance in the Jovian aurora from Juno-UVS spectral images. *Journal of Geophysical*
458 *Research: Space Physics*, n/a(n/a), e2020JA028142. <https://doi.org/10.1029/2020JA028142>

459 Gjerloev, J. W., Hoffman, R. A., Friel, M. M., Frank, L. A., & Sigwarth, J. B. (2004). Substorm behavior of the
460 auroral electrojet indices. *Annales Geophysicae*, 22(6), 2135–2149. [https://doi.org/10.5194/angeo-22-2135-](https://doi.org/10.5194/angeo-22-2135-2004)
461 2004

462 Gjerloev, J. W., Hoffman, R. A., Sigwarth, J. B., & Frank, L. A. (2007). Statistical description of the bulge-type
463 auroral substorm in the far ultraviolet. *Journal of Geophysical Research: Space Physics*, 112(A7).
464 <https://doi.org/10.1029/2006JA012189>

465 Gjerloev, J. W., Hoffman, R. A., Sigwarth, J. B., Frank, L. A., & Baker, J. B. H. (2008). Typical auroral substorm:
466 A bifurcated oval. *Journal of Geophysical Research: Space Physics*, 113(A3).
467 <https://doi.org/10.1029/2007JA012431>

468 Gladstone, G. R., Persyn, S. C., Eterno, J. S., Walther, B. C., Slater, D. C., Davis, M. W., et al. (2017). The
469 Ultraviolet Spectrograph on NASA's Juno Mission. *Space Science Reviews*, 213(1), 447–473.
470 <https://doi.org/10.1007/s11214-014-0040-z>

471 Gray, R. L., Badman, S. V., Bonfond, B., Kimura, T., Misawa, H., Nichols, J. D., et al. (2016). Auroral evidence of
472 radial transport at Jupiter during January 2014. *Journal of Geophysical Research: Space Physics*, 121(10),
473 9972–9984. <https://doi.org/10.1002/2016JA023007>

474 Greathouse, T. K., Gladstone, G. R., Davis, M. W., Slater, D. C., Versteeg, M. H., Persson, K. B., et al. (2013).
475 Performance results from in-flight commissioning of the Juno Ultraviolet Spectrograph (Juno-UVS). In
476 *UV, X-Ray, and Gamma-Ray Space Instrumentation for Astronomy XVIII* (Vol. 8859, p. 88590T).
477 International Society for Optics and Photonics. <https://doi.org/10.1117/12.2024537>

478 Grodent, D., Gérard, J.-C., Clarke, J. T., Gladstone, G. R., & Waite, J. H. (2004). A possible auroral signature of a
479 magnetotail reconnection process on Jupiter. *Journal of Geophysical Research: Space Physics*, *109*(A5).
480 <https://doi.org/10.1029/2003JA010341>

481 Grodent, Denis, Bonfond, B., Yao, Z., Gérard, J.-C., Radioti, A., Dumont, M., et al. (2018). Jupiter's Aurora
482 Observed With HST During Juno Orbits 3 to 7. *Journal of Geophysical Research: Space Physics*, *123*(5),
483 3299–3319. <https://doi.org/10.1002/2017JA025046>

484 Gustin, J., Cowley, S. W. H., Gérard, J.-C., Gladstone, G. R., Grodent, D., & Clarke, J. T. (2006). Characteristics of
485 Jovian morning bright FUV aurora from Hubble Space Telescope/Space Telescope Imaging Spectrograph
486 imaging and spectral observations. *Journal of Geophysical Research: Space Physics*, *111*(A9).
487 <https://doi.org/10.1029/2006JA011730>

488 Hameiri, E., Laurence, P., & Mond, M. (1991). The ballooning instability in space plasmas. *Journal of Geophysical*
489 *Research: Space Physics*, *96*(A2), 1513–1526. <https://doi.org/10.1029/90JA02100>

490 Henderson, M. G. (2009). Observational evidence for an inside-out substorm onset scenario. *Annales Geophysicae*,
491 *27*(5), 2129–2140. <https://doi.org/10.5194/angeo-27-2129-2009>

492 Hue, V., Gladstone, G. R., Greathouse, T. K., Kammer, J. A., Davis, M. W., Bonfond, B., et al. (2019). In-flight
493 Characterization and Calibration of the Juno-ultraviolet Spectrograph (Juno-UVS). *The Astronomical*
494 *Journal*, *157*(2), 90. <https://doi.org/10.3847/1538-3881/aafb36>

495 Kalmoni, N. M. E., Rae, I. J., Watt, C. E. J., Murphy, K. R., Samara, M., Michell, R. G., et al. (2018). A diagnosis of
496 the plasma waves responsible for the explosive energy release of substorm onset. *Nature Communications*,
497 *9*(1), 4806. <https://doi.org/10.1038/s41467-018-07086-0>

498 Kimura, T., Nichols, J. D., Gray, R. L., Tao, C., Murakami, G., Yamazaki, A., et al. (2017). Transient brightening of
499 Jupiter's aurora observed by the Hisaki satellite and Hubble Space Telescope during approach phase of the
500 Juno spacecraft. *Geophysical Research Letters*, *44*(10), 4523–4531. <https://doi.org/10.1002/2017GL072912>

501 Kronberg, E. A., Woch, J., Krupp, N., Lagg, A., Khurana, K. K., & Glassmeier, K.-H. (2005). Mass release at
502 Jupiter: Substorm-like processes in the Jovian magnetotail. *Journal of Geophysical Research: Space*
503 *Physics*, *110*(A3). <https://doi.org/10.1029/2004JA010777>

504 Kronberg, E. A., Glassmeier, K.-H., Woch, J., Krupp, N., Lagg, A., & Dougherty, M. K. (2007). A possible intrinsic
505 mechanism for the quasi-periodic dynamics of the Jovian magnetosphere. *Journal of Geophysical*
506 *Research: Space Physics*, 112(A5). <https://doi.org/10.1029/2006JA011994>

507 Kullen, A., & Karlsson, T. (2004). On the relation between solar wind, pseudobreakups, and substorms. *Journal of*
508 *Geophysical Research: Space Physics*, 109(A12). <https://doi.org/10.1029/2004JA010488>

509 Liou, K., Newell, P. T., Zhang, Y.-L., & Paxton, L. J. (2013). Statistical comparison of isolated and non-isolated
510 auroral substorms. *Journal of Geophysical Research: Space Physics*, 118(5), 2466–2477.
511 <https://doi.org/10.1002/jgra.50218>

512 Louarn, P., Roux, A., Perraut, S., Kurth, W. S., & Gurnett, D. A. (2000). A study of the Jovian “energetic
513 magnetospheric events” observed by Galileo: role in the radial plasma transport. *Journal of Geophysical*
514 *Research: Space Physics*, 105(A6), 13073–13088. <https://doi.org/10.1029/1999JA900478>

515 Louarn, P., Paranicas, C. P., & Kurth, W. S. (2014). Global magnetodisk disturbances and energetic particle
516 injections at Jupiter. *Journal of Geophysical Research: Space Physics*, 119(6), 4495–4511.
517 <https://doi.org/10.1002/2014JA019846>

518 Lui, A. T. Y., Chang, C.-L., Mankofsky, A., Wong, H.-K., & Winske, D. (1991). A cross-field current instability for
519 substorm expansions. *Journal of Geophysical Research: Space Physics*, 96(A7), 11389–11401.
520 <https://doi.org/10.1029/91JA00892>

521 Manners, H., Masters, A., & Yates, J. N. (2018). Standing Alfvén Waves in Jupiter’s Magnetosphere as a Source of
522 ~10- to 60-Min Quasiperiodic Pulsations. *Geophysical Research Letters*, 45(17), 8746–8754.
523 <https://doi.org/10.1029/2018GL078891>

524 Masters, A. (2017). Model-Based Assessments of Magnetic Reconnection and Kelvin-Helmholtz Instability at
525 Jupiter’s Magnetopause. *Journal of Geophysical Research: Space Physics*, 122(11), 11,154–11,174.
526 <https://doi.org/10.1002/2017JA024736>

527 Mauk, B., & Bagenal, F. (2013). Comparative Auroral Physics: Earth and Other Planets. In *Auroral Phenomenology*
528 *and Magnetospheric Processes: Earth And Other Planets* (pp. 3–26). American Geophysical Union
529 (AGU). <https://doi.org/10.1029/2011GM001192>

530 Mauk, B. H., Williams, D. J., & McEntire, R. W. (1997). Energy-time dispersed charged particle signatures of
531 dynamic injections in Jupiter's inner magnetosphere. *Geophysical Research Letters*, *24*(23), 2949–2952.
532 <https://doi.org/10.1029/97GL03026>

533 Miyashita, Y., & Ieda, A. (2018). Revisiting substorm events with preonset aurora. *Annales Geophysicae*, *36*(5),
534 1419–1438. <https://doi.org/10.5194/angeo-36-1419-2018>

535 Mura, A., Adriani, A., Altieri, F., Connerney, J. E. P., Bolton, S. J., Moriconi, M. L., et al. (2017). Infrared
536 observations of Jovian aurora from Juno's first orbits: Main oval and satellite footprints. *Geophysical
537 Research Letters*, *44*, 5308–5316. <https://doi.org/10.1002/2017GL072954>

538 Murphy, K. R., Mann, I. R., Rae, I. J., Walsh, A. P., & Frey, H. U. (2014). Inner magnetospheric onset preceding
539 reconnection and tail dynamics during substorms: Can substorms initiate in two different regions? *Journal
540 of Geophysical Research: Space Physics*, *119*(12), 9684–9701. <https://doi.org/10.1002/2014JA019795>

541 Nichols, J. D., Clarke, J. T., Gérard, J. C., Grodent, D., & Hansen, K. C. (2009). Variation of different components
542 of Jupiter's auroral emission. *Journal of Geophysical Research (Space Physics)*, *114*(A13), A06210.
543 <https://doi.org/10.1029/2009JA014051>

544 Nishimura, Y., Lyons, L., Zou, S., Angelopoulos, V., & Mende, S. (2010). Substorm triggering by new plasma
545 intrusion: THEMIS all-sky imager observations. *Journal of Geophysical Research: Space Physics*,
546 *115*(A7). <https://doi.org/10.1029/2009JA015166>

547 Nishimura, Y., Lyons, L. R., Angelopoulos, V., Kikuchi, T., Zou, S., & Mende, S. B. (2011). Relations between
548 multiple auroral streamers, pre-onset thin arc formation, and substorm auroral onset. *Journal of
549 Geophysical Research: Space Physics*, *116*(A9). <https://doi.org/10.1029/2011JA016768>

550 Oberhagemann, L. R., & Mann, I. R. (2020). A New Substorm Onset Mechanism: Increasingly Parallel Pressure
551 Anisotropic Ballooning. *Geophysical Research Letters*, *47*(2), e2019GL085271.
552 <https://doi.org/10.1029/2019GL085271>

553 Pulkkinen, T. I., Baker, D. N., Wiltberger, M., Goodrich, C., Lopez, R. E., & Lyon, J. G. (1998). Pseudobreakup and
554 substorm onset: Observations and MHD simulations compared. *Journal of Geophysical Research: Space
555 Physics*, *103*(A7), 14847–14854. <https://doi.org/10.1029/97JA03244>

556 Radioti, A., Grodent, D., Gérard, J.-C., Vogt, M. F., Lystrup, M., & Bonfond, B. (2011). Nightside reconnection at
557 Jupiter: Auroral and magnetic field observations from 26 July 1998. *Journal of Geophysical Research:*
558 *Space Physics*, 116(A3). <https://doi.org/10.1029/2010JA016200>

559 Radioti, A., Grodent, D., Gérard, J.-C., Bonfond, B., Gustin, J., Pryor, W., et al. (2013). Auroral signatures of
560 multiple magnetopause reconnection at Saturn. *Geophysical Research Letters*, 40(17), 4498–4502.
561 <https://doi.org/10.1002/grl.50889>

562 Radioti, A., Yao, Z., Grodent, D., Palmaerts, B., Roussos, E., Dialynas, K., et al. (2019). Auroral Beads at Saturn
563 and the Driving Mechanism: Cassini Proximal Orbits. *The Astrophysical Journal*, 885(1), L16.
564 <https://doi.org/10.3847/2041-8213/ab4e20>

565 Sergeev, V. A., Kornilova, T. A., Kornilov, I. A., Angelopoulos, V., Kubyshkina, M. V., Fillingim, M., et al. (2010).
566 Auroral signatures of the plasma injection and dipolarization in the inner magnetosphere. *Journal of*
567 *Geophysical Research: Space Physics*, 115(A2). <https://doi.org/10.1029/2009JA014522>

568 Tao, C., Kataoka, R., Fukunishi, H., Takahashi, Y., & Yokoyama, T. (2005). Magnetic field variations in the Jovian
569 magnetotail induced by solar wind dynamic pressure enhancements. *Journal of Geophysical Research:*
570 *Space Physics*, 110(A11). <https://doi.org/10.1029/2004JA010959>

571 Vasylunas, V. M. (1983). Physics of the Jovian magnetosphere. In A. J. Dessler (Ed.), *Physics of the Jovian*
572 *Magnetosphere* (pp. 395–453). Cambridge University Press.

573 Vogt, M. F., Kivelson, M. G., Khurana, K. K., Joy, S. P., & Walker, R. J. (2010). Reconnection and flows in the
574 Jovian magnetotail as inferred from magnetometer observations. *Journal of Geophysical Research: Space*
575 *Physics*, 115(A6). <https://doi.org/10.1029/2009JA015098>

576 Vogt, M. F., Bunce, E. J., Kivelson, M. G., Khurana, K. K., Walker, R. J., Radioti, A., et al. (2015). Magnetosphere-
577 ionosphere mapping at Jupiter: Quantifying the effects of using different internal field models. *Journal of*
578 *Geophysical Research: Space Physics*, 120(4), 2584–2599. <https://doi.org/10.1002/2014JA020729>

579 Vogt, M. F., Gyalay, S., Kronberg, E. A., Bunce, E. J., Kurth, W. S., Zieger, B., & Tao, C. (2019). Solar Wind
580 Interaction With Jupiter’s Magnetosphere: A Statistical Study of Galileo In Situ Data and Modeled
581 Upstream Solar Wind Conditions. *Journal of Geophysical Research: Space Physics*, 124(12), 10170–
582 10199. <https://doi.org/10.1029/2019JA026950>

583 Woch, J., Krupp, N., & Lagg, A. (2002). Particle bursts in the Jovian magnetosphere: Evidence for a near-Jupiter
584 neutral line. *Geophysical Research Letters*, 29(7), 42-1-42-4. <https://doi.org/10.1029/2001GL014080>
585 Yao, Z., Pu, Z. Y., Rae, I. J., Radioti, A., & Kubyshkina, M. V. (2017). Auroral streamer and its role in driving
586 wave-like pre-onset aurora. *Geoscience Letters*, 4(1), 8. <https://doi.org/10.1186/s40562-017-0075-6>
587 Yao, Z., Bonfond, B., Clark, G., Grodent, D., Dunn, W. R., Vogt, M. F., et al. (2020). Reconnection and
588 Dipolarization Driven Auroral Dawn Storms and Injections. *Earth and Space Science Open Archive*.
589 <https://doi.org/10.1002/essoar.10503657.1>
590 Zhang, B., Delamere, P. A., Yao, Z., Bonfond, B., Lin, D., Sorathia, K. A., et al. (2020). How Jupiter's Unusual
591 Magnetospheric Topology Structures Its Aurora. *ArXiv E-Prints*, 2006, arXiv:2006.14834.
592

593 Data

594 The data included herein are either archived in NASA's Planetary Data System ([http://pds-](http://pds-atmospheres.nmsu.edu/data_and_services/atmospheres_data/JUNO/juno.html)
595 [atmospheres.nmsu.edu/data_and_services/atmospheres_data/JUNO/juno.html](http://pds-atmospheres.nmsu.edu/data_and_services/atmospheres_data/JUNO/juno.html)). This research is
596 also based on publicly available observations acquired with the NASA/ESA Hubble Space
597 Telescope and obtained at the Space Telescope Science Institute, which is operated by AURA
598 for NASA (<https://archive.stsci.edu/hst/search.php>). Data analysis was performed with the
599 AMDA science analysis system provided by the Centre de Données de la Physique des Plasmas
600 (CDPP) supported by CNRS, CNES, Observatoire de Paris and Université Paul Sabatier,
601 Toulouse. The THEMIS data are available from <http://themis.ssl.berkeley.edu/data/themis/>. The
602 IMAGE-WIC images can be accessed at <https://spdf.gsfc.nasa.gov/pub/data/image/fuv/> and were
603 processed using the FUVIEW3 software (<http://sprg.ssl.berkeley.edu/image/>).

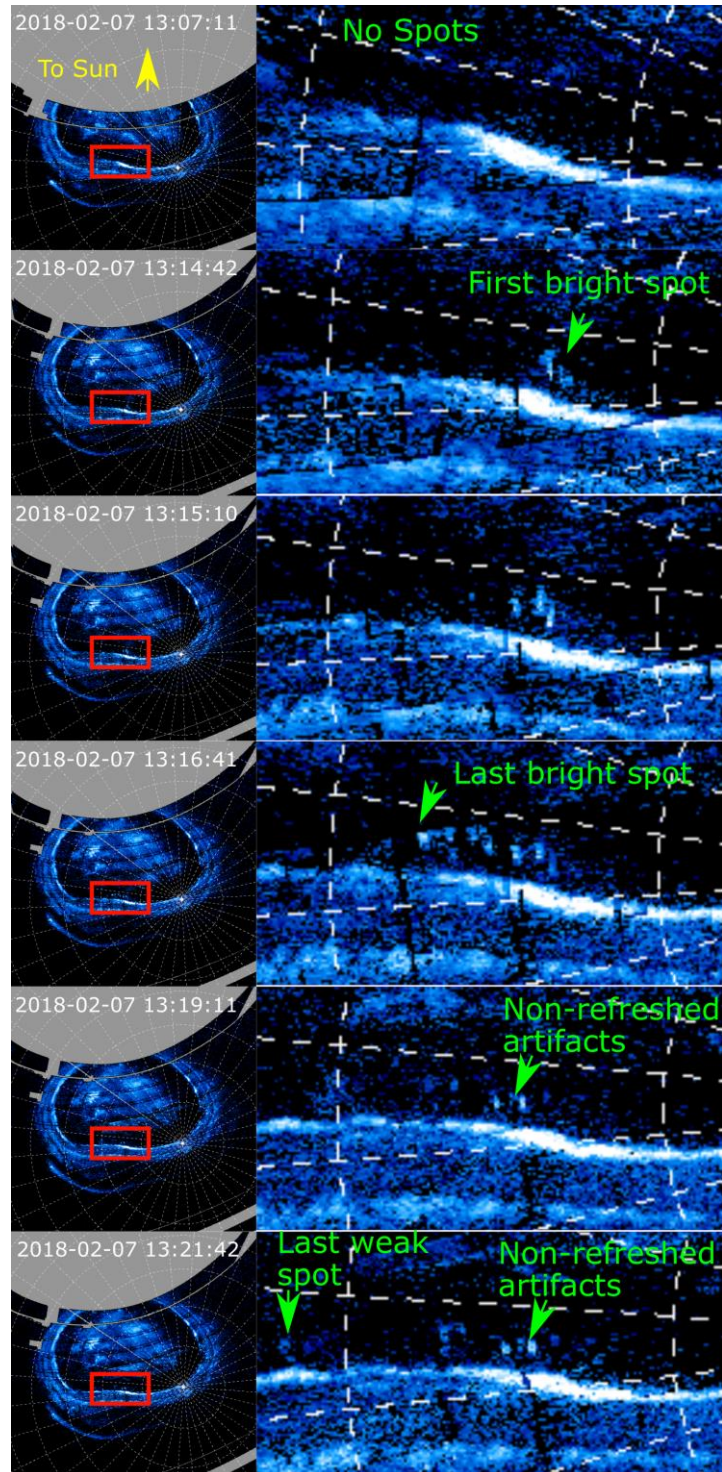
604

605 Acknowledgments

606 The authors are grateful to J.E.P. Connerney for helpful discussions concerning the manuscript.
607 B.B. is a Research Associate of the Fonds de la Recherche Scientifique - FNRS. We are grateful
608 to NASA and contributing institutions which have made the Juno mission possible. This work
609 was funded by NASA's New Frontiers Program for Juno via contract with the Southwest
610 Research Institute. B.B., D.G., J.-C.G., and J.M. acknowledge financial support from the Belgian
611 Federal Science Policy Office (BELSPO) via the PRODEX Programme of ESA. The research at
612 the University of Iowa was supported by NASA through Contract 699041X with Southwest
613 Research Institute.

614 Supplementary Materials:

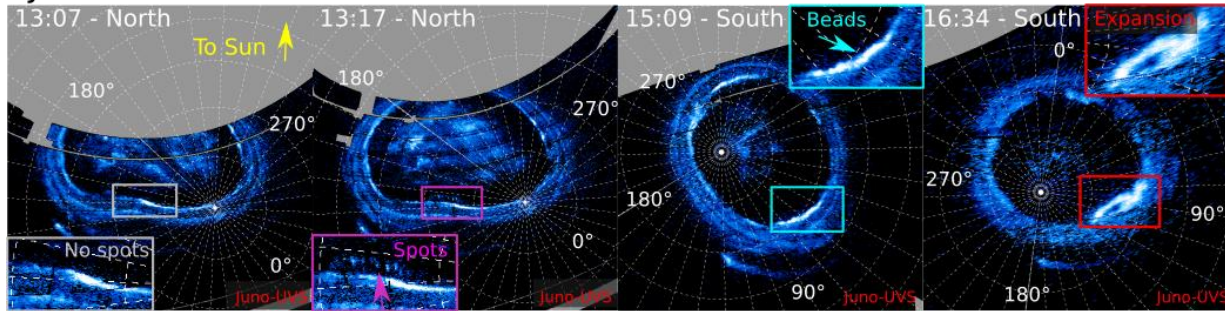
615 Figures S1-S9



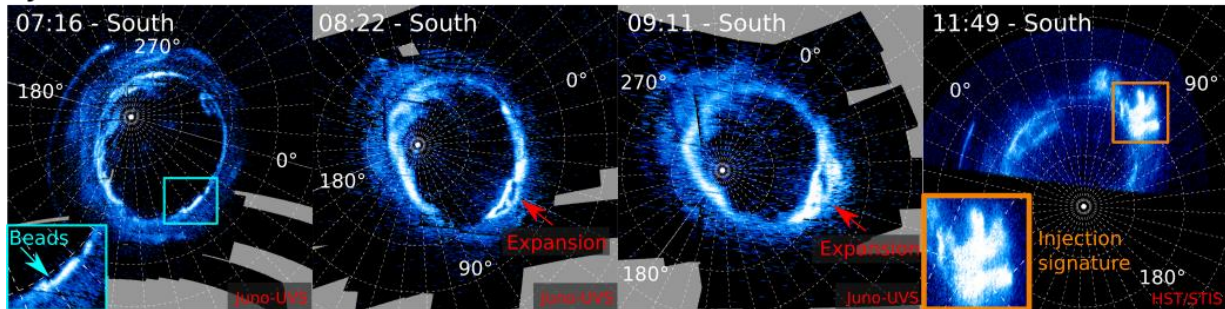
617
 618
 619
 620
 621
 622
 623
 624

Figure 1. Details of the development of the transient spots during the PJ11 dawn storm. A polar projection of the whole northern aurora is shown on the left and a zoom on the region boxed in red is shown on the right. The Sun direction is towards the top and dashed lines show System III meridians and planetocentric parallel spaced every 10° . Bright spots of the size of the instrument at PSF successively appeared from dawn to dusk, approximately 1000 km apart. The two bright spots remaining on the center of the last two frames are due to the non-refreshment of this part of the image.

PJ11



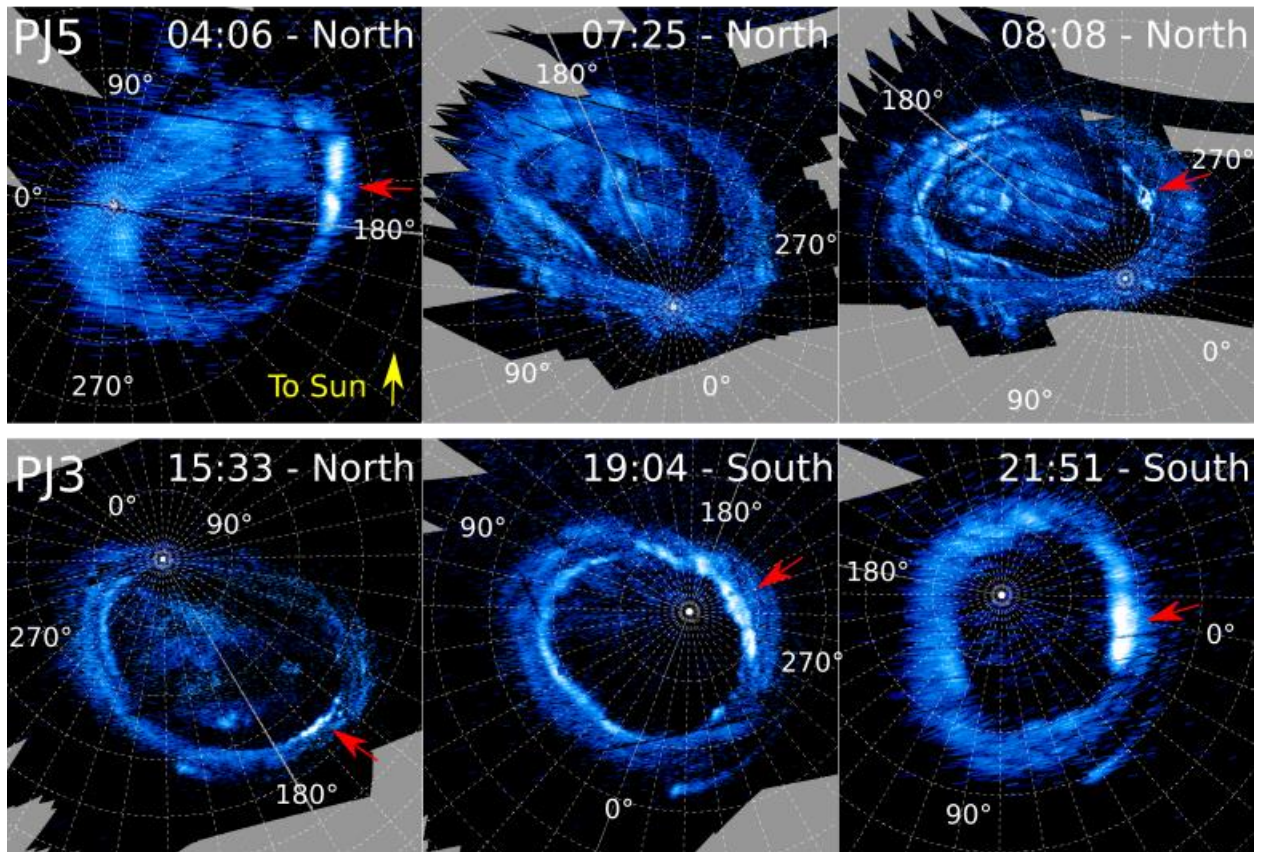
PJ6



625
626
627
628
629
630
631
632
Figure 2. Polar projection of the development of a dawn storm, based on observations acquired by Juno-UVS and HST/STIS during the 11th and the 6th perijove sequences. On PJ11, the event was preceded by the progressive appearance of a set of transient spots poleward of the main emission. Two hours later, the dawn storm itself started as an enhancement of the main emission in the form of beads before the arc began to fork and expand, both latitudinally and longitudinally. On the PJ6 sequence, the same sequence of emergence of beads, followed by the expansion phase is observed, but subsequent observations by both Juno-UVS and HST-STIS show that the equatorward arc transforms into a large injection signature.

633

Non-Isolated Dawn Storms



635

636

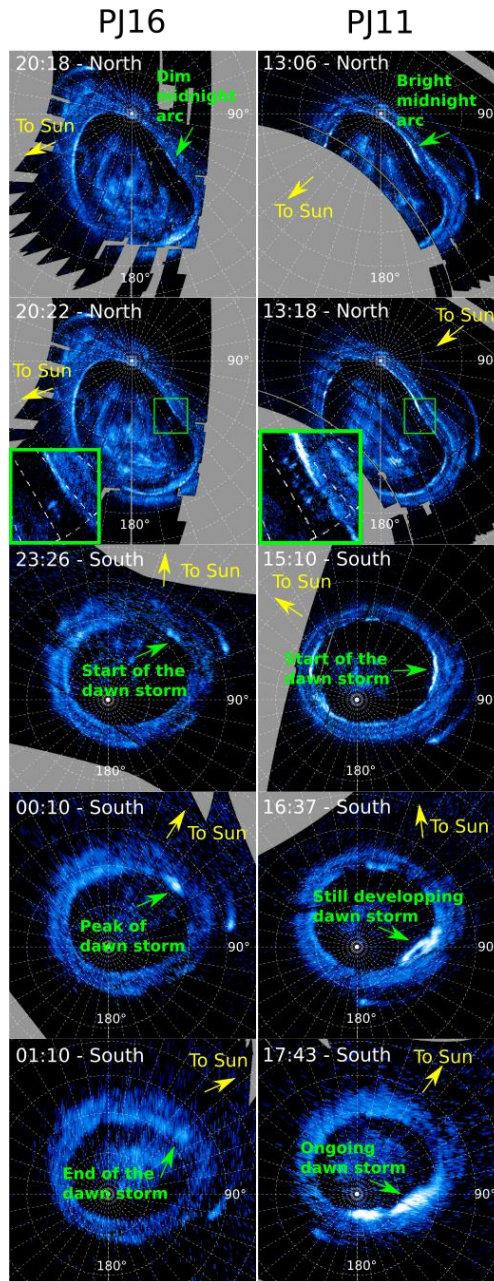
637

638

Figure 3. Polar projections of the development of non-isolated dawn storms during PJ3 and PJ5. The red arrow highlights the dawn storms. During PJ5, a second dawn storm took place ~3 hours after the first one. On PJ3, new dawn storms seem to appear during all the southern branch of the perijove sequence.

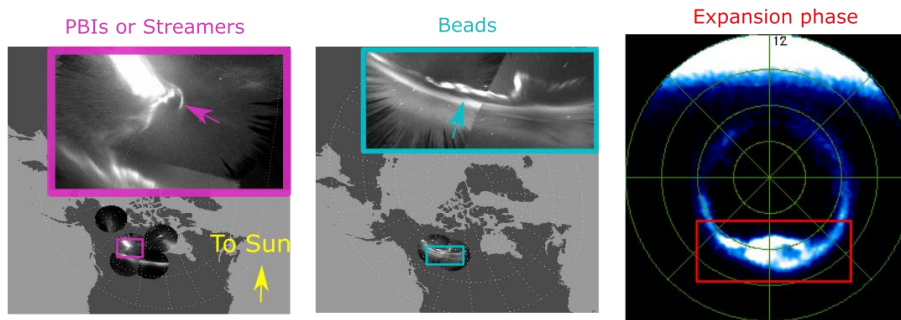
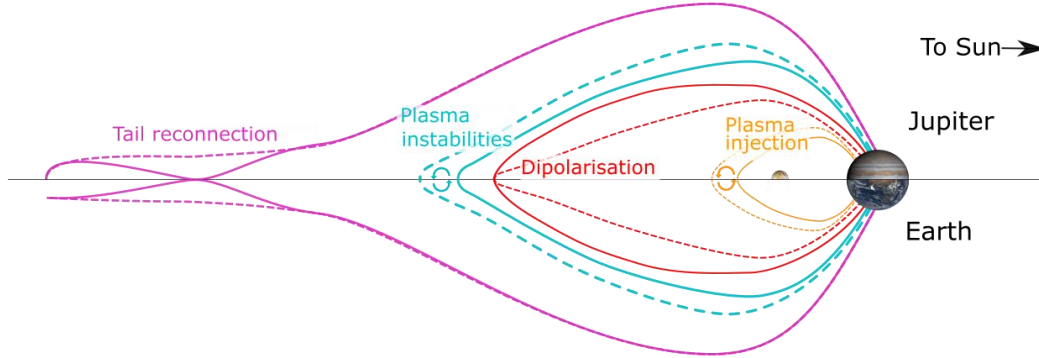
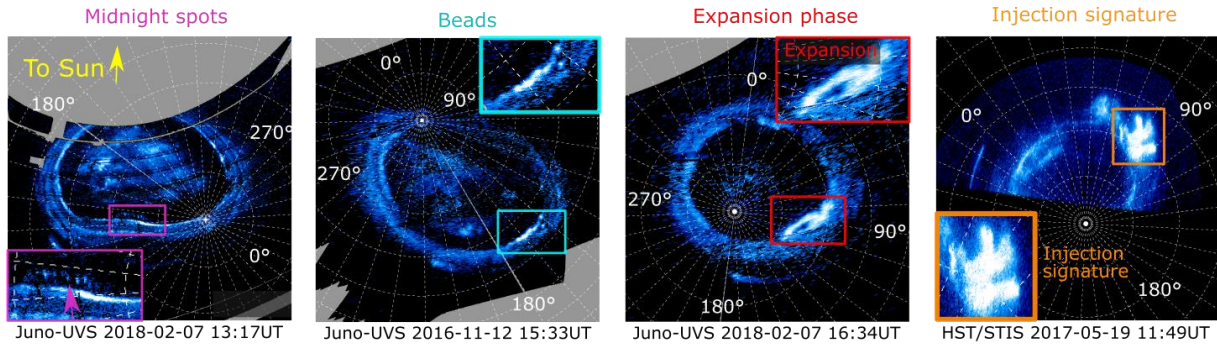
639

640



641
642
643
644
645

Figure 4. The left column shows polar projections of the aurorae during the 16th perijove, and the right column shows a similar sequence for the 11th perijove. While the sequence on PJ11 compares with a terrestrial substorm (Fig. 1-2), the one on PJ16 is much more limited in size, emitted power and duration and would be more similar to a terrestrial pseudo-breakup.



Themis all-sky cam. 2008-02-29 08:20UT Themis all-sky cam. 2008-01-29 08:33UT Image/WIC 2001-01-14 03:59UT

Figure 5. Polar projections of the UV aurora showing four different phases of a Jovian dawn storm: 1) the short lived polar midnight spots, 2) the formation of irregularities on the main emission pre-dawn part 3) the expansion phase, with the two arcs splitting and 4) the injection signatures in the outer emission. The first three images are based on data from the Juno-UVS instrument and the fourth one comes from Hubble Space Telescope observations carried out to support Juno. These four phases appear to correspond to nightside tail reconnection, plasma instabilities, current disruption/dipolarization in the middle magnetosphere and to flux tube interchange, respectively, as illustrated in the general scheme shown in the central scheme (not to scale). These auroral features corresponding to these phases in the terrestrial aurora are show on the bottom row. In the bottom, the first two images come from the THEMIS network of all-sky cameras (Nishimura et al., 2010; Yao et al., 2017). The third image corresponds to Earth's aurora as seen from IMAGE-WIC.

657
658

659
660

	date	Peak power (W)	Identified features
PJ1	27 Aug 2016 18:00 => 20:00		b?, e
PJ3	11 Dec 2016 15:10 = > 22:02	$8.1 \cdot 10^{11}$	b, e, g, nids
PJ5	27 Mar 2017 3:56 => 06:00 7 :33=> 11 :09	$1.5 \cdot 10^{11}$ $1.1 \cdot 10^{11}$	e, g, i, nids
PJ6	19 May 2017 07:14 => 10:54	$1.6 \cdot 10^{12}$	b?, e, i
PJ7	10 Jul 2017 22:43 => 00:00	$2.7 \cdot 10^{11}$	e, i
PJ9	24 Oct 2017 12:19 => 13:50	$6.0 \cdot 10^{11}$	e
PJ11	07 Feb 2018 12:58 => 18:49	$8.5 \cdot 10^{11}$	s, b, e, g
PJ14	16 Jul 2018 08:42=> 10:15	$6.5 \cdot 10^{11}$	e
PJ16	29 Oct 2018 23:20=> 01:00	$1.4 \cdot 10^{11}$	s, e, i?
PJ20	29 May 2019 09 :30 => 12 :54	$9.2 \cdot 10^{11}$	e, g, i

661 **Table 1.** List of the dawn storms identified during Juno's perijove observations sequences. The second column
662 collects the approximate times of the expansion phases of the dawn storm. The end time in particular are
663 approximate, as there is no clear criterion for when the phenomenon is finished. Start and end times in bold indicate
664 that the observations started or ended at the indicated time, but the dawn storm probably lasted longer. The third
665 column indicates the peak power reached by the dawn storm and the fourth column indicates the observed feature
666 during this sequence, (s) meaning the spots, (b) the beads, (e) the expansion, (g) the gap, (i) the injections and (nids)
667 the occurrence of non-isolated dawn storms. The PJ1 dawn storm started after the end of the UVS observations, but
668 the beginning of the expansion phase was observed with the JIRAM (Jovian InfraRed Auroral Mapper) instrument
669 (Adriani et al., 2017; Mura et al., 2017) (Figure S9).
670